Hindawi
Mathematical Problems in Engineering
Volume 2018, Article ID 7054385, 20 pages
https://doi.org/10.1155/2018/7054385

Research Article

Energy-Efficient Enhancement for Viscoelastic Injection Rheomolding Using Hierarchy Orthogonal Optimization

Jinghua Xu, Tiantian Wang, Shuyou Zhang, and Jianrong Tan

State Key Laboratory of Fluid Power and Mechatronic Systems, Zhejiang University, Hangzhou, China

Correspondence should be addressed to Shuyou Zhang; zsy@zju.edu.cn

Received 2 March 2018; Revised 4 July 2018; Accepted 11 July 2018; Published 23 August 2018

Academic Editor: Yannis Dimakopoulos

The viscoelastic injection molding involves multidisciplinary thermoplastic rheomolding parameters which is a complex mathematical problem. Particularly for rheomolding of complex parts with thin-walled structure, boss, and grooves, the increasing higher requirements on energy efficiency and rheomolding quality are put forward. Therefore, an energy-efficient enhancement method for viscoelastic injection molding using hierarchy orthogonal optimization (HOO) is proposed. Based on the thermoplastic rheomolding theory and considering the viscoelastic effects in injection molding, a set of partial differential equations (PDE) describing the physical coupling behavior of the mold-melt-injection molding machine is established. The fuzzy sliding mode control (FSMC) is used to reduce the energy consumption in the control system of the injection molding machine's clamping force. Then, the HOO model of viscoelastic injection rheomolding is built in terms of thermoplastic rheomolding parameters and injection machine parameters. In initial hierarchy, through Taguchi orthogonal experiment and Analysis of Variance (ANOVA), the amount of gate, melt temperature, mold temperature, and packing pressure are extracted as the significant influence parameters. In periodical hierarchy, the multiobjective optimization model takes the forming time, warping deformation, and energy consumption of injection molding as the multiple objectives. The NSGA-II (Nondominated Sorting Genetic Algorithm II) optimization is employed to obtain the optimal solution through the global Pareto front. In ultimate hierarchy, three candidate schemes are compared on multiple objectives to determine the final energy-efficient enhancement scheme. A typical temperature controller part is analyzed and the energy consumption of injection molding is reduced by 41.85%. Through the physical experiment of injection process, the proposed method is further verified.

1. Introduction

The viscoelastic injection molding involves multidisciplinary thermoplastic rheomolding parameters which is a complex mathematical problem. Particularly for rheomolding of complex parts with thin-walled structure, boss, and grooves, the increasing higher requirements on energy efficiency and rheomolding quality are put forward. The most common methods for forming plastic polymers include injection, compression, extrusion, coextrusion, blow, and blend molding. Injection-molded parts are widely used in consumer products and industrial equipment, the injection-molded components constitute 42% and 33% in toys and medical equipment components, respectively [1].

In the field of theoretical research, Khayat et al. [2] proposed an adaptive (Lagrangian) boundary element approach for the general two-dimensional simulation of confined moving-boundary flow of viscous incompressible fluids. Araújo et al. [3] described the development of a parallel three-dimensional unstructured nonisothermal flow solver for the simulation of the injection molding process. Kwon et al. [4] proposed a novel approach to predict anisotropic shrinkage of amorphous polymers in injection moldings based on PVT equation of state, frozen-in molecular orientation, and elastic recovery. Yang et al. [5] proposed a numerical simulation algorithm for the complicated filling process with edge effect in the process of resin transfer molding. The electrohydraulic servo system is adopted in the injection molding machine; it is an important research direction for the hydraulic injection molding machine to improve the servo control performance and energy saving capability [6]. The clamping force F is controlled indirectly by means of the pressure control of the

clamping cylinder via a servo valve. Because the clamping force control requires high pressure, low flow, low power, and low energy efficiency, the energy efficiency is low in the traditional injection molding machine. Therefore, this paper optimizes the traditional clamping force control system by fuzzy sliding mode control algorithm [6–8].

In the field of experimental research, Xu et al. [9] performed a series of numerical simulation to examine the influence of thermal history experienced during injection molding on the plastic deformation and fracture energy of PC specimens. Mold temperature is an important process parameter that affects microinjection molding quality. Huang et al. [10] investigated the effects of high mold surface temperature generated by induction heating in enhancing the replication rate of microfeatures of LGPs. Kusić et al. [11] investigated the influence of six injection molding process parameters on the postmolding shrinkage and warping of parts made from polypropylene filled with calcium carbonate, by carrying out experimental tests using the Taguchi method; the best combination of process parameters was found.

In the research of energy consumption and green rheomolding, Fernandez et al. [12] developed a methodology for the rheological testing of polymers during the injection molding process, this method has been designed to consider the nonconventional features of the plastication phase that result from the injection of recycled thermoplastics. Vera-Sorroche et al. [13] showed that polymer rheology had a significant effect on process energy consumption and thermal homogeneity of the melt. Tsai et al. [14] presents pragmatic techniques for mechatronic design and injection speed control of an ultra-high-speed plastic injection molding machine. It provides useful references for engineers and practitioners attempting to design pragmatic, low-cost but high-performance ultra-high-injection speed controllers. Studer and Ehrig [15] proposed a numerical procedure to reduce the material amount required for injection-molded parts by optimizing their wall thickness distributions with respect to part quality and identifying an upper limit for the injection pressure.

In the field of simulation and multiobjective optimization research, Baltussen et al. [16] used numerical simulation to study the viscoelastic flow front instability and developed a two-phase viscoelastic model in two dimensions which predicts a fountain flow instability and is able to monitor this instability in the full nonlinear regime. Kanagalakshmi et al. [17] proposed a multimodel-based proportional integral derivative (PID) control scheme in real-time and the simulation studies of the PID, fuzzy, and adaptive neurofuzzy inference system (ANFIS) control schemes, which mainly contributes to the barrel temperature control. Shie [18] proposed a hybrid method integrating a trained generalized regression neural network (GRNN) and a sequential quadratic programming (SQP) method to determine an optimal parameter setting of the injection molding process. Zhai et al. [19] proposed a computationally efficient scheme based on flow path to locate the optimum gate for achieving balanced flow; the range of filling time is employed as objective function. Liu et al. [20] presented a set of procedures for the optimization of IMPP, the multiple-objective optimization was performed by applying the nondominated sorting genetic algorithm (NSGA-II), optimization results indicate that the optimization method has high accuracy.

As the viscoelastic injection molding involves multidisciplinary thermoplastic rheomolding heterogeneous parameters, it is difficult to implement optimization for the traditional multiobjective optimization. Therefore, Hierarchy orthogonal optimization (HOO) method is proposed to solve numerous heterogeneous parameters optimization. The paper is the deepening and extension of our previous work [21–27]. The aim of the paper is to improve the energy efficiency and molding part quality by matching molding equipment, tooling equipment, and mold from vast heterogeneous parameters.

2. Theoretical Model of Viscoelastic Injection Rheomolding Using Governing Equations

2.1. Thermoplastic Fluid considering Viscoelastic Effects in Channel. Injection molding is a process in which granular polymer, usually thermoplastic, is fed from a hopper into a heated barrel where it is melted, after which a screw or ram forces the material into a mold. Pressure is maintained until the part has hardened. The mold is opened and the part is ejected by some mechanism. It is by far the most important technique for mass production. The major disadvantages of the process are that not all polymers can be processed (most thermosets), and the metal molds are very expansive. This basic process is also used for coinjection of two different polymers. There are two extrusion barrels and injection systems. A shot is made with one polymer, and a second shot with a second polymer can be used to surround or surface the part made in the first shot. Coinjection is often done to achieve a cosmetic effect or to alter use properties. Another variation of injection molding is structural foam molding. The mold is only partially filled, and injected plastic expands to fill the mold to produce a part that is light weight because of the entrapped porosity, but the skin is integral. Foamed polymers have lower weight (and cost) over their nonfoamed counterparts, and the mechanical properties are often comparable. This process is often used on polyphenylene oxide, olefins, vinyls, nylons, and thermoplastic elastomers.

The viscoelastic effects of polymer play dominant role in injection molding which affects significantly the quality of the final molding product. Viscoelasticity is the property of materials exhibiting both viscous and elastic characteristics when undergoing deformation. In the process of injection molding, the polymer is heated into molten state and injected into the mold cavity under the action of external pressure and finally cooled and solidified. The molecular chain of polymer fluid produces large shear deformation and tensile deformation, which has the characteristics of viscoelasticity. In general, polymer fluid is non-Newtonian fluid and its viscosity and other physical parameters will vary with the change of shear-stress, temperature, and pressure. The viscoelastic nature of the polymer results in development of shear and normal stresses and large elastic deformation during filling with subsequent incomplete relaxation during

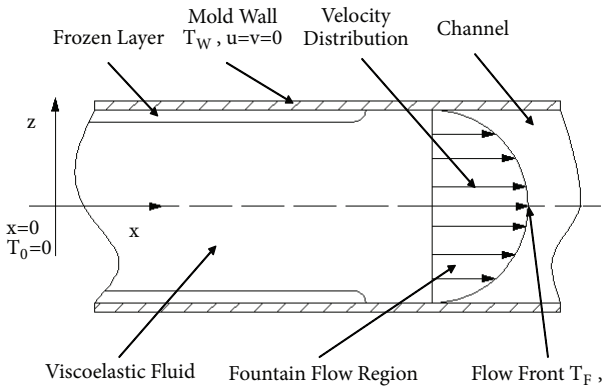

Figure 1: Thermoplastic rheomolding during viscoelastic injection.

the cooling stage [28]. It will cause defects in products, such as excessive residual stress and incomplete filling. Therefore, the study of flows of viscoelastic liquids is a very important research area. It is very difficult to numerically simulate the effects of viscoelastic fluid in the flow channel, but there are some very important contributions to the field [29–32]. Nickell et al. [29] proposed a numerical solution for solving incompressible, viscous free-surface problems for Newtonian fluid. The experiments results showed Newtonian jet expands about 13% which is substantial agreement with the proposed method. Dimakopoulos [30] proposed the parallelization of a fully implicit and stable finite element algorithm which can be applied to calculate simulation of time-dependent, free-surface flows of multimode viscoelastic liquids. Hadid et al. [31] developed a viscoelastic model based on a simple power law with stress-dependent parameters. The proposed model demonstrates high stress sensitivity. Pettas et al. [32] employed mixed finite element method combined with an elliptic grid generator to account for the deformable shape of the interface which and used the Phan–Thien–Tanner (PTT) model to account for the viscoelasticity of the material.

Multiphase flow is important in many industrial processes: injection molding, riser reactors, bubble column reactors, fluidized bed reactors, scrubbers, dryers, etc. Multiphase flow regimes include bubbly flow, droplet flow, particle-laden flow, slug flow, annular flow, stratified flow, free-surface flow, oscillatory flow, and irrotational flow. The part forming methods contains rheomolding, thixomolding, thixocasting, cold chamber, hot chamber, semisolid, press forming, etc. The flow model of polymer melt in the flow channel is usually simplified to two-dimensional flow, which is widely studied [33–35]. Thermoplastic rheomolding during injection is shown in Figure 1.

The governing equations are the conservation of the mass, the momentum, and the energy, as written as follows:

Continuity equation:

$$\frac{\partial \rho}{\partial t} + \frac{\partial (\rho u)}{\partial x} + \frac{\partial (\rho v)}{\partial y} + \frac{\partial (\rho w)}{\partial z} = 0 \tag{1}$$

Momentum equation:

$$\begin{aligned}
\rho\left(\frac{\partial u}{\partial t} + u\frac{\partial u}{\partial x} + v\frac{\partial u}{\partial z} + w\frac{\partial u}{\partial z}\right) + \frac{\partial P}{\partial x} &= \eta\nabla^2 u + g_x\rho \\
\rho\left(\frac{\partial v}{\partial t} + u\frac{\partial v}{\partial x} + v\frac{\partial v}{\partial z} + w\frac{\partial v}{\partial z}\right) + \frac{\partial P}{\partial y} &= \eta\nabla^2 v + g_y\rho \\
\rho\left(\frac{\partial w}{\partial t} + u\frac{\partial w}{\partial x} + v\frac{\partial w}{\partial z} + w\frac{\partial w}{\partial z}\right) + \frac{\partial P}{\partial z} &= \eta\nabla^2 w + g_z\rho
\end{aligned} \tag{2}$$

Energy equation:

$$\rho C_p\left(\frac{\partial T}{\partial t} + u\frac{\partial T}{\partial x} + v\frac{\partial T}{\partial y} + w\frac{\partial T}{\partial z}\right) = \eta\nabla^2 T + Q_c \tag{3}$$

where ∇ is Hamilton operator; u, v, w are component of velocity vector V in x, y, z directions ($\mathrm{m\cdot s^{-1}}$); ρ is melt density of material ($\mathrm{g\cdot cm^{-3}}$); C_p is specific heat capacity($\mathrm{J\cdot kg^{-1}\cdot {}^\circ C^{-1}}$); η is kinetic viscosity of the material (Pa·s); P is pressure (MPa); g_x, g_y, g_z are acceleration of gravity in x, y, z directions ($\mathrm{m\cdot s^{-2}}$); T is melt temperature (°C); Q_c is internal calorific (J).

The n-th order reaction kinetics (Kamal model) is used to calculate the curing behavior of a thermoset material in a reactive molding, microchip encapsulation or underfill encapsulation analysis. The n-th order reaction kinetics model is given by the equations:

$$\begin{aligned}
\frac{d\alpha}{dt} &= \left(K_1 + K_2\alpha^m\right)(1-\alpha)^h \\
K_1 &= A_1 \exp\left(-\frac{E_1}{T}\right) K_2 = A_2 \exp\left(-\frac{E_2}{T}\right)
\end{aligned} \tag{4}$$

where α is the degree of cure (0, 1); T is melt temperature (°C); t is time(s); m, h, A_1, A_2, E_1, E_2 are constants.

2.2. Simplified Control Equations. The flow of fluid plastic in mold cavity is very complicated. If physical phenomena are expressed by mathematical models, some hypothesis need to be put forward to simplify the flow model. Some basic hypothesis are as follows [36]:

(1) Neglecting the velocity in the direction of the thickness.

(2) The heat conduction in the flow direction is relatively small and the heat convection is relatively smal.

(3) The velocity orientation in the plane is smaller than that in the thickness direction of the plate and can be ignored.

(4) Neglecting the heat generated by compression.

(5) Neglecting the heat generated internally.

(6) The material is incompressible, neglecting the viscoelastic heating of the material, the specific heat C_p, and the thermal conductivity k of the melt are constants.

According to the above hypothesis, (1), (2), and (3) can be simplified and the formulas can be obtained.

$$\frac{\partial \rho}{\partial t} + \frac{\partial (\rho u)}{\partial x} + \frac{\partial (\rho v)}{\partial y} = 0 \tag{5}$$

$$\begin{aligned} \frac{\partial P}{\partial x} &= \eta \frac{\partial u}{\partial z} \\ \frac{\partial P}{\partial y} &= \eta \frac{\partial v}{\partial z} \end{aligned} \tag{6}$$

$$\rho C_p \left(\frac{\partial T}{\partial t} + u \frac{\partial T}{\partial x} + v \frac{\partial T}{\partial y} \right) = k \frac{\partial^2 T}{\partial z^2} + \eta \dot{\gamma}^2 \tag{7}$$

$$\dot{\gamma} = \sqrt{\left(\frac{\partial u}{\partial z} \right)^2 + \left(\frac{\partial v}{\partial z} \right)^2} \tag{8}$$

where u, v are component of velocity vector V in x, y direction ($\mathrm{m \cdot s^{-1}}$); ρ is melt density of material ($\mathrm{g \cdot cm^{-3}}$); C_p is specific heat capacity($\mathrm{J \cdot kg^{-1} \cdot {}^\circ C^{-1}}$); η is kinetic viscosity of the material (Pa·s); k is thermal conductivity($\mathrm{W \cdot m^{-1} \cdot {}^\circ C^{-1}}$); T is melt temperature (°C); $\dot{\gamma}$ is strain rate tensor intensity ($\mathrm{s^{-1}}$); P is pressure (MPa).

The modified cross-model is adopted in the viscosity model. It is suitable for the viscosity in both the Newtonian-plateau and shear-thinning behavior of the melt.

$$\eta = \frac{\eta_0}{1 + \left(\eta_0 \dot{\gamma} / \tau^* \right)^{1-a}} \tag{9}$$

where η_0 is zero shear-rate kinetic viscosity (Pa·s); η is kinetic viscosity of the material (Pa·s); $\dot{\gamma}$ is strain rate tensor intensity ($\mathrm{s^{-1}}$); τ^* is the critical shear-stress that is need to transform the melt flow from the Newtonian to shear-thinning or power-law behavior (Pa); a is the measure of degree of the shear-thinning behavior.

$$\eta_0 = B \cdot \exp \left[\frac{-A_3 \left(T - T_g \right)}{A_4 + \left(T - T_g \right)} \right] \tag{10}$$

where B, A_3, A_4 are material constants; T_g is the sensitivity of zero shear viscosity to temperature (°C); T is melt temperature (°C).

2.3. Numerical Solution of Pressure Field. The flow of the melt in the mold cavity is affected by the shape of the mold cavity. When calculating the pressure field of the melt flow, some initial conditions need to be known. Based on the established model, the initial conditions and boundary conditions of the melt flow are as follows [37]:

(1) Entrance of the channel

$$T = T_0 \tag{11}$$

(2) Center of flow channel

$$\frac{\partial u}{\partial z} = \frac{\partial v}{\partial z} = 0 \tag{12}$$

(3) On the mold wall

$$\begin{aligned} u &= v = 0 \\ \frac{\partial T}{\partial y} &= \frac{\partial T}{\partial z} = k \left(T - T_w \right) \\ T &= T_w \end{aligned} \tag{13}$$

where T_0 is temperature of injection (°C); T_w is mold temperature (°C); T is melt temperature (°C); k is thermal conductivity($\mathrm{W \cdot m^{-1} \cdot {}^\circ C^{-1}}$); u, v are component of velocity vector V in x, y direction ($\mathrm{m \cdot s^{-1}}$).

The finite element method is used to solve the continuity equation and the momentum equation to obtain the pressure field [38].

(1) After the triangular mesh is divided, the pressure in the grid can be represented by linear interpolation.

$$P(x, y) = \sum_{j=1}^{3} P_j N_j \tag{14}$$

where N_j is linear interpolating function; P_j is node pressure in trigonometric unit (MPa); P is pressure (MPa); j is corresponding node position.

(2) The Galerkin-finite element method is used to discretize the pressure control field. The reasonable function is selected from the boundary condition and the inlet boundary condition, so that the pressure front boundary condition is $P = 0$.

$$\begin{pmatrix} K_{aa} & K_{ab} \\ K_{ab} & K_{bb} \end{pmatrix} \begin{pmatrix} P_f \\ 0 \end{pmatrix} = \begin{pmatrix} Q_f \\ Q_m \end{pmatrix} \tag{15}$$

where $\boldsymbol{K}$ is stiffness matrix; P is pressure (MPa); Q is flow rate ($\mathrm{cm^3 \cdot s^{-1}}$);

(3) The corresponding boundary conditions are as follows: the pressure at the flow front is $P = 0$, the flow velocity at the entrance point is known, and the flow velocity of the already filled node is 0. Bring boundary conditions into (6), (7), (14), and (15); each node pressure can be solved by super relaxation iterative method.

2.4. Numerical Solution of Temperature Field. There are some important temperatures in the process of melt flow, such as the flow front temperature T_F, the bulk temperature T_B, and the bulk temperature at end of fill T_E. The following are simply given their qualitative description and calculation. Flow front temperature T_F is the middle flow temperature when a polymer melt is filled with a node. Because it represents the temperature of the center of the melt. Bulk temperature T_B in the thermal fluid is a convenient reference point for evaluating properties related to convective heat transfer, particularly in applications related to flow in pipes and ducts. The concept of the bulk temperature T_B is that adiabatic mixing of the fluid from a given cross section of the duct will result in some equilibrium temperature that accurately reflects the average temperature of the moving fluid, more so than a simple average like the film temperature.

Bulk temperature at end of filling T_E is the result of a single set of data, which is a good reflection of the temperature change in the mold filling. It describes the location of energy in transmission, and the change of polymer melt temperature is not only in time and location, but also due to the different thickness during the whole injection molding.

(1) Solving temperature control equation by Finite Difference Method (FDM). Differential separation grid is introduced into the wall thickness and flow direction of the cavity. When solving the simplified energy equation (7), in each time step, the convection heat transfer term and the viscous dissipation term can be calculated from the previous time step. In the new time step, they can be regarded as known heat sources.

$$\rho C_p \left(\left[\frac{\partial T}{\partial t} \right]_i^n + \left[u \frac{\partial T}{\partial x} + v \frac{\partial T}{\partial y} \right]_i^n \right) = \left[k \frac{\partial^2 T}{\partial z^2} \right]_i^n + \left[\eta \dot{\gamma}^2 \right]_i^{n-1} \tag{16}$$

where u, v are component of velocity vector V in x, y direction ($\mathrm{m \cdot s^{-1}}$); ρ is melt density of material ($\mathrm{g \cdot cm^{-3}}$); C_p is specific heat capacity ($\mathrm{J \cdot kg^{-1} \cdot {}^\circ C^{-1}}$); η is kinetic viscosity of the material (Pa·s); k is thermal conductivity($\mathrm{W \cdot m^{-1} \cdot {}^\circ C^{-1}}$), T is melt temperature (°C); $\dot{\gamma}$ is strain rate tensor intensity ($\mathrm{s^{-1}}$); n is iteration step; i is node sequence.

(2) The temperature's derivative of time is interpolated by forward. Central difference of the heat conduction term along the direction derivative of the thickness [39]. The equation is obtained.

$$\frac{\partial T}{\partial t} = \frac{T_i^{n+1} - T_i^n}{\Delta t}$$
$$\frac{\partial^2 T}{\partial z^2} = \frac{T_{i+1}^{n+1} - 2T_i^{n+1} + T_{i-1}^{n+1}}{(\Delta z)^2} \tag{17}$$

(3) Finally, bring boundary conditions into (16) and (17); each node temperature calculation column can be obtained.

$$\boldsymbol{M_a} \cdot \boldsymbol{T^{n+1}} = \boldsymbol{b} \tag{18}$$

where $\boldsymbol{M_a}$ is coefficient matrix; $\boldsymbol{T^{n+1}}$ is temperature of node at new time (°C), which is equal to T_F; $\boldsymbol{b}$ is temperature at the last time and the heat source related to the convection heat transfer and the viscous heat (°C).

Combined with the corresponding temperature boundary conditions, the temperature distribution at the different boundaries of the die is given; the above equation is solved by Gauss-Seidel method.

The melt will produce force on the moving die side under the effect of filling pressure P, and the clamping mechanism is needed to balance the force to avoid the leakage of the melt. This force can be calculated by the formula

$$\nabla \boldsymbol{\sigma} + F = 0 \tag{19}$$

where ∇ is Hamilton operator; $\boldsymbol{\sigma}$ is total stress (MPa); F is clamping force (N).

Table 1: Physical parameters of ABS.

Material Type	ABS
Melt density of material ρ ($\mathrm{g \cdot cm^{-3}}$)	0.96971
Solid density of material ρ_s ($\mathrm{g \cdot cm^{-3}}$)	1.07500
Specific heat capacity C_p ($\mathrm{J \cdot kg^{-1} \cdot {}^\circ C^{-1}}$)	2400
Thermal conductivity k ($\mathrm{W \cdot m^{-2} \cdot {}^\circ C^{-1}}$)	0.18

3. Hierarchy Orthogonal Optimization Model of Viscoelastic Injection Rheomolding

The hierarchy orthogonal optimization (HOO) model of viscoelastic injection rheomolding is built in terms of thermoplastic rheomolding parameters and injection machine parameters.

3.1. Thermoplastic Rheomolding Parameters. The parameters of the injection molding process determine the quality of the product, including temperature, pressure, time, and injection molding machine model.

The usual injection mold has a gating system; after the injection molding is completed, these parts of the material will cause the waste of raw materials. Reasonable design of the gating system is important for energy saving and emission reduction. The material utilization R can represent this feature; the higher the material utilization rate, the more reasonable the gating system.

$$R = \frac{M_1}{M_0} \quad R \in (0, 1) \tag{20}$$

where R is material utilization ratio; M_1 is total weight of parts (g); M_0 is total mass (g).

Volumetric shrinkage V_s refers to the percentage difference between the size of the product at the molding temperature and the difference between the size of the product and the cooling from the mold to room temperature. It reflects the extent of the size reduction after the product is removed from the mold.

$$V_s = \frac{V_1 - V_3}{V_1} \quad V_s \in (0, 1) \tag{21}$$

where V_s is volumetric shrinkage; V_1 is cavity volume of part ($\mathrm{cm^3}$); V_3 is part volume after cooling ($\mathrm{cm^3}$).

The model material is ABS, and its physical parameters are listed in Table 1.

3.2. Injection Machine Parameters. The key equipment of injection molding is injection molding machine, while the utilization efficiency of injection molding machine is less than 50%. Therefore, the research on reducing the energy consumption of injection molding machine is in line with the requirements of green production.

(1) Injection speed v_i

$$v_i = \frac{4Q}{\pi D^2} \tag{22}$$

where v_i is injection speed ($cm \cdot s^{-1}$); Q is flow rate ($cm^3 \cdot s^{-1}$); D is screw diameter (cm).

(2) Screw metering stroke L

The screw metering stroke is calculated according to the model and the volume of the gating system.

$$L = \frac{4V_0\rho_s}{\pi D^2 \rho} \tag{23}$$

where L is screw metering stroke (cm); V_0 is total volume (cm^3); D is screw diameter (cm); ρ_s is solid density of materials ($g \cdot cm^{-3}$); ρ is melt density of material ($g \cdot cm^{-3}$).

(3) Clamping force F control system

In research [40–42], the control strategy of hydraulic system in injection molding process is basically controlled by fuzzy sliding mode control (FSMC). This control strategy can force the control system to slide according to the predetermined state of sliding mode according to the current state of the control system in dynamic process.

The relationship between the flow of the hydraulic pump and the speed of the pump is expressed by

$$q_1 = CN_sV \tag{24}$$

where q_1 is hydraulic fluid flow ($cm^3 \cdot s^{-1}$); C is volume efficiency of hydraulic pump; V is rated displacement of a quantitative pump ($cm^3 \cdot s^{-1}$); N_s is motor speed ($r \cdot min^{-1}$).

The flow balance equation for the hydraulic cylinder is

$$q_1 = \lambda P_1 + \frac{V_4(h)}{K}\frac{\partial P_1}{\partial t} + A_1\frac{\partial H}{\partial t} \tag{25}$$

where A_1 is effective area of hydraulic cylinder (cm^{-2}); P_1 is hydraulic pressure (MPa); H is displacement of hydraulic cylinder (cm); λ is total leakage coefficient of hydraulic cylinder; K is volume modulus of hydraulic fluid (MPa); V_4 is total volume of front and rear of hydraulic cylinder (cm^3).

The equation of force balance for the motion of a hydraulic cylinder is

$$F = A_1P_1 = M_E\frac{\partial^2 h}{\partial t^2} + C_1\frac{\partial H}{\partial t} + k_eH + F_L \tag{26}$$

where F is clamping force (N); M_E is equivalent mass of hydraulic cylinder (Kg); C_1 is viscous damping coefficient of hydraulic cylinder ($N \cdot s \cdot cm^{-1}$); k_e is load elastic coefficient ($N \cdot cm^{-1}$); F_L is load resistance (N).

(4) Energy consumption of injection molding W

According to the working mechanism of the screw injection molding machine, the screw moves along the direction of the barrel and does not consider the power required by the heating. The energy consumption in the plasticizing process is mainly derived from the torque produced by the rotation of the screw of the injection molding machine [43]. So, we can get the formula for the energy consumption of injection molding W of the injection molding machine.

$$N_m = \frac{2\pi r M_n}{60} = QP \tag{27}$$

$$W = N_m t \tag{28}$$

where N_m is power consumption of screw rotation (W); r is screw speed ($r \cdot min^{-1}$); M_n is screw torque (N·m); W is energy consumption of injection molding (J); t is time (s); Q is flow rate ($cm^3 \cdot s^{-1}$); P is pressure (MPa).

3.3. Taguchi Orthogonal Experiment and Analysis of Variance in Initial Hierarchy. There are many heterogeneous injection process parameters which affect the quality of final injection product, such as the amount of gate N_g, melt temperature T, mold temperature T_W, injection pressure P_{in}, packing pressure P_p, packing time t_p, and cooling time t_c. In this paper, seven parameters above are selected as design parameters according to the practical production experience. A large number of experiments must be carried out to determine the degree of influence of these process parameters on the quality of the molding products, so as to facilitate the subsequent parameter optimization. The Taguchi method was taken as the DOE (Design of Experiments) method for the L_{18} (3^7) orthogonal experiment. Taguchi method is a reliable technology in statistics and has been proved to be reliable. The method uses orthogonal arrays to study a large number of variables through a small number of experiments which can achieve high quality without increasing cost [44, 45]. The experimental results can be measured by signal-to-noise ratio (SNR), as shown in

$$SN = -10\log_{10}\frac{\sum_{i=1}^{n} Y_i^2}{n} \tag{29}$$

where SN is signal-to-noise ratio; n is the number of experiment, here $n = 1$; Y_i is experimental result.

Take temperature controller, for example, the injection molding process parameters and their initial levels are listed in Table 2. After the initial values are set, eighteen schemes are simulated, respectively. The calculated results (including forming time t_0, warping deformation w_r and energy consumption of injection molding W) are listed in Table 3. In the eighteen experiments, the minimum of t_0 is number 9: A=4, B=240, C=50, D=140, E=90, F=5, G=20, $t_0 = 36.40$ s; the minimum of w_r is number 15: A=2, B=240, C=50, D=120, E=100, F=10, G=15, $w_r = 0.1306$ mm; the minimum of W is number 6: A=2, B=240, C=70, D=100, E=80, F=10, G=20, $W = 135.9094$ J. Analysis of Variance (ANOVA) of t_0, w_r, W is listed in Tables 4–6, respectively. The analysis results show that the corresponding P-value is not more than 0.05, indicating a significant impact on the objectives, which must be considered in the optimization process [20]. Of the seven parameters, the most significant effect on forming time is A and C; the most significant effect on warping deformation is A, B, and E; the most significant effect on energy consumption of injection molding is A and B. t_0, w_r, W have the smaller-the-better characteristic. The

Table 2: Injection molding process parameters of the Taguchi orthogonal experiment.

Initial Parameters	Level 1	Level 2	Level 3
A: the amount of gate N_g	1	2	4
B: melt temperature T (°C)	220	230	240
C: mold temperature T_W (°C)	50	60	70
D: injection pressure P_{in} (MPa)	100	120	140
E: packing pressure P_p (MPa)	80	90	100
F: packing time t_p (s)	5	10	15
G: cooling time t_c (s)	15	20	25

Table 3: Experimental results of the Taguchi orthogonal experiment.

Number	Injection molding process parameters							Experiment results		
	A	B	C	D	E	F	G	t_0(s)	w_r(mm)	W(J)
1	1	220	50	100	80	5	15	38.89	0.1550	295.9368
2	1	230	60	120	90	10	20	45.51	0.1477	265.2554
3	1	240	70	140	100	15	25	55.26	0.1431	240.896
4	2	220	50	120	90	15	25	42.86	0.1373	173.0041
5	2	230	60	140	100	5	15	45.11	0.1319	152.2613
6	2	240	70	100	80	10	20	54.74	0.1399	135.9094
7	4	220	60	100	100	10	25	40.17	0.1478	206.751
8	4	230	70	120	80	15	15	48.54	0.1512	185.9026
9	4	240	50	140	90	5	20	36.40	0.1395	172.3589
10	1	220	70	140	90	5	15	52.01	0.1506	287.7244
11	1	230	50	100	100	10	20	40.26	0.1437	267.9215
12	1	240	60	120	80	15	25	47.01	0.1462	243.2058
13	2	220	60	140	80	15	20	44.36	0.1420	170.538
14	2	230	70	100	90	5	25	53.61	0.1400	149.981
15	2	240	50	120	100	10	15	40.99	0.1306	138.8948
16	4	220	70	120	100	5	20	47.17	0.1452	204.1483
17	4	230	50	140	80	10	25	38.29	0.1477	188.9207
18	4	240	60	100	90	15	15	41.40	0.1436	188.9207

main effects plots for SN ratios are shown in Figures 2(a), 2(b), and 2(c) which further show the degrees effect of the seven parameters on the three objectives. Therefore, it can be concluded that among the seven injection molding process parameters which have significant influence on the molding products are A, B, C, and E (the amount of gate N_g, melt temperature T, mold temperature T_W, and packing pressure P_p).

3.4. Multiobjective Optimization Model Using NSGA-II in Periodical Hierarchy. There are many factors affecting the molding precision of the products, such as the injection process parameters, the manufacturing precision of the mold, the material performance, and the selection of the injection molding machine. Therefore, it is necessary to establish a multiobjective optimization model and consider many factors as possible to find out the optimal solution to improve the precision of the product. Multiobjective optimization of injection molding process parameters has a very important impact on green manufacturing and energy saving. Deb et al. [46] proposed a Nondominated Sorting Genetic Algorithm II (NSGA-II) with $O(MN^2)$ (where M is the number of objectives and N is the population size) computational complexity. It can alleviate all the follow three difficulties in multiobjective evolutionary algorithms (EAs): (1) $O(MN^3)$ computational complexity; (2) nonelitism approach; (3) the need for specifying a sharing parameter. NSGA-II is widely used to solve the multiobjective optimization problems in injection molding process [47–49]. Wei et al. [47] used NSGA-II method to solve the complex multiobjective optimal performance design of large-scale injection molding machines. The experiment results show that the method is effective and practical. Zhang and Ma [48] developed a multiobjective optimal model considering minimization of production cost and minimization of operation cost based on NSGA-II and covariance matrix adaptation evolution strategy (CMA-ES). Yang et al. [49] proposed a new multiobjective optimization method for sheet metal part based on the

Table 4: ANOVA result for forming time t_0.

Data source	Degrees of freedom	Sum of squares	Mean squares	F-value	P-value
A	2	89.829	44.915	46.81	0.005
B	2	5.386	2.693	2.81	0.206
C	2	419.497	209.749	218.62	0.001
D	2	0.782	0.391	0.41	0.697
E	2	0.998	0.499	0.52	0.640
F	2	1.861	0.930	0.97	0.473
G	2	6.499	3.250	3.39	0.170
Error	3	2.878	0.959	—	—
Total	17	580.732	—	—	—

Table 5: ANOVA result for warping deformation w_r.

Data source	Degrees of freedom	Sum of squares	Mean squares	F-value	P-value
A	2	0.000397	0.000198	80.53	0.002
B	2	0.000099	0.000049	20.06	0.018
C	2	0.000026	0.000013	5.31	0.103
D	2	0.000014	0.000007	2.91	0.198
E	2	0.000118	0.000059	23.99	0.014
F	2	0.000004	0.000002	0.72	0.557
G	2	0.000004	0.000002	0.80	0.528
Error	3	0.000007	0.000002	—	—
Total	17	0.000689	—	—	—

support vector regression (SVR) surrogate model and NSGA-II in order to solve multiple conflicting objectives during the optimization process.

In order to solve the complex multiobjective optimal performance design of parameters, NSGA-II is used to find a much better spread of design solutions and better convergence near the true Pareto-optimal front [50–52]. After obtaining the pressure field and the temperature field, the multiobjective optimization model (MOO) of the quality of the injection molding products is further established. According to the orthogonal experimental results shown in Section 3.3, the amount of gate N_g, melt temperature T, mold temperature T_W, and packing pressure P_p are extracted as the four main performance evaluation parameters in NSGA-II, taking total forming time t_0, warping deformation w_r, and energy consumption of injection molding W as the optimization objectives. The multiobjective optimization model can be formulated as

$$\begin{aligned} \text{Find:} \quad & \boldsymbol{x} = \left[N_g, T, T_W, P_p\right] \\ \text{Minimize:} \quad & f(\boldsymbol{x}) = \left\{t_0(\boldsymbol{x}), w_r(\boldsymbol{x}), W(\boldsymbol{x})\right\} \\ \text{Subject to:} \quad & \begin{cases} 1 \le N_g \le 4 \\ 220^\circ\text{C} \le T \le 240^\circ\text{C} \\ 50^\circ\text{C} \le T_W \le 70^\circ\text{C} \\ 80MPa \le P_p \le 100MPa \end{cases} \end{aligned} \tag{30}$$

where N_g is the amount of gate; T is melt temperature (°C); T_W is mold temperature (°C); P_p is packing pressure (MPa); t_0 is forming time (s); w_r is warping deformation (mm); W is energy consumption of injection molding (J); $\boldsymbol{x}$ are parameters of injection process, including N_g, T, T_W, P_p; $f(\boldsymbol{x})$ is objective function $\{t_0(\boldsymbol{x}), w_r(\boldsymbol{x}), W(\boldsymbol{x})\}$ considering parameters $\boldsymbol{x}$ of injection process.

Minor changes of the design parameters may tremendously affect the unitary performance of products. NSGA-II changes the domination rules to reveal design constraint condition, which can avoid unsteady factor of penalty coefficient value in penalty function approach [47]. The overall impact hierarchy structure is established based on the multiobjective system model. Then the feedback effects of each parameter on the overall precision are calculated. The algorithm process of NSGA-II is shown in Figure 3. Initial species colony P including N individuals values are random in the bounding range. The theoretical calculation steps of NSGA-II are as follows:

(1) According to the optimization objectives and constraints, the species colony is sorted and the crowding distance is calculated.

(2) Then the intermediate species colony is generated through league matches-choosing, crossover, and mutation. Intermediate species colony combines with initial species colony.

(3) The calculated sorting and species groups can be generated by selecting N individuals [47].

There are many kinds of parameter combinations and uncertain search space since the four parameter ranges are

Table 6: ANOVA result for energy consumption of injection molding W.

Data source	Degrees of freedom	Sum of squares	Mean squares	F-value	P-value
A	2	40011.1	20005.6	1193.17	0.001
B	2	3605.5	1802.7	107.52	0.002
C	2	73.0	36.5	2.18	0.261
D	2	118.3	59.2	3.53	0.163
E	2	59.0	29.5	1.76	0.312
F	2	7.3	3.6	0.22	0.816
G	2	193.3	96.7	5.76	0.094
Error	3	50.3	16.8	—	—
Total	17	44539.5	—	—	—

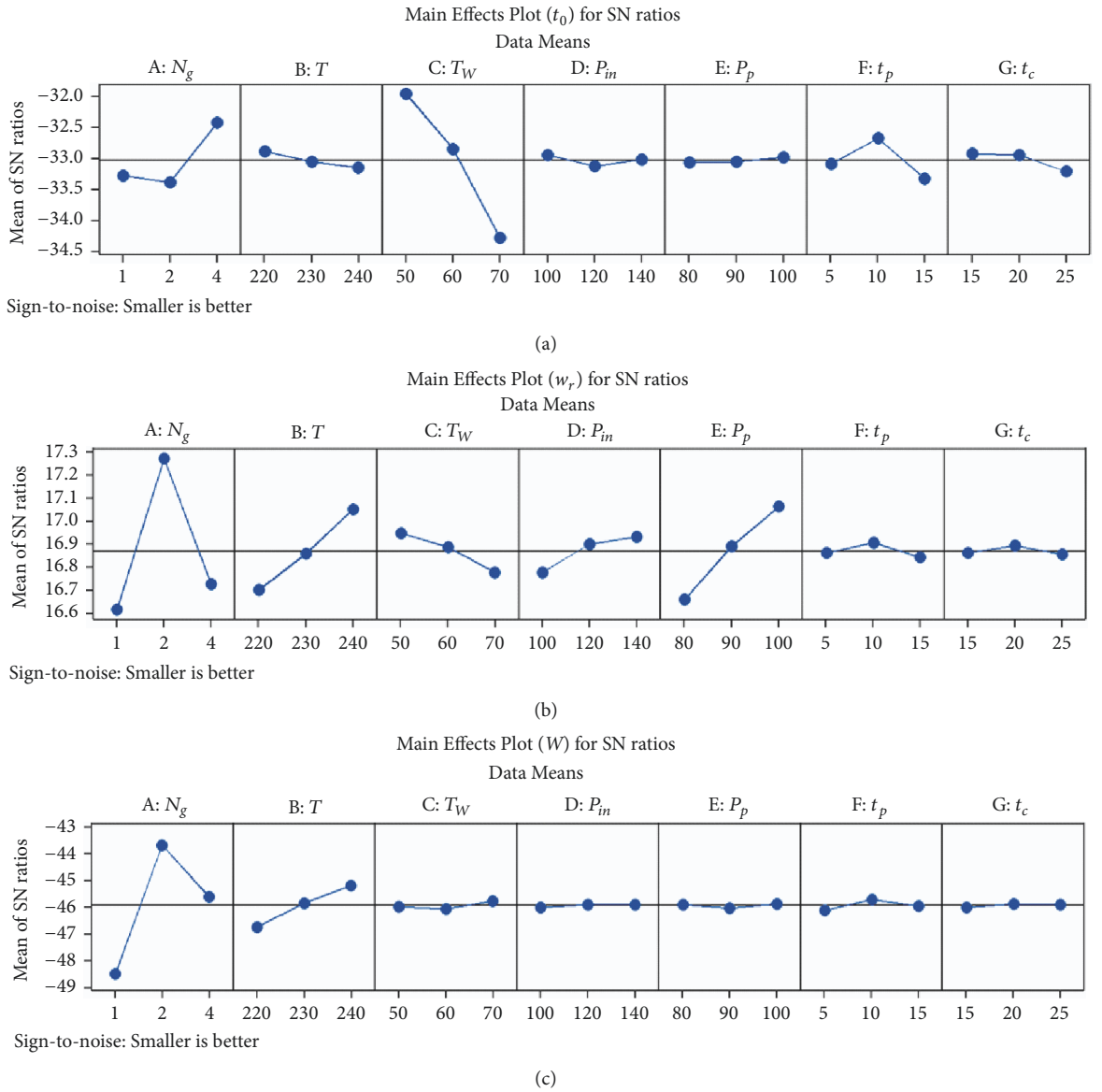

Figure 2: Main effects plots for SN ratios, (a) forming time t_0; (b) warping deformation w_r; (c) energy consumption of injection molding W.

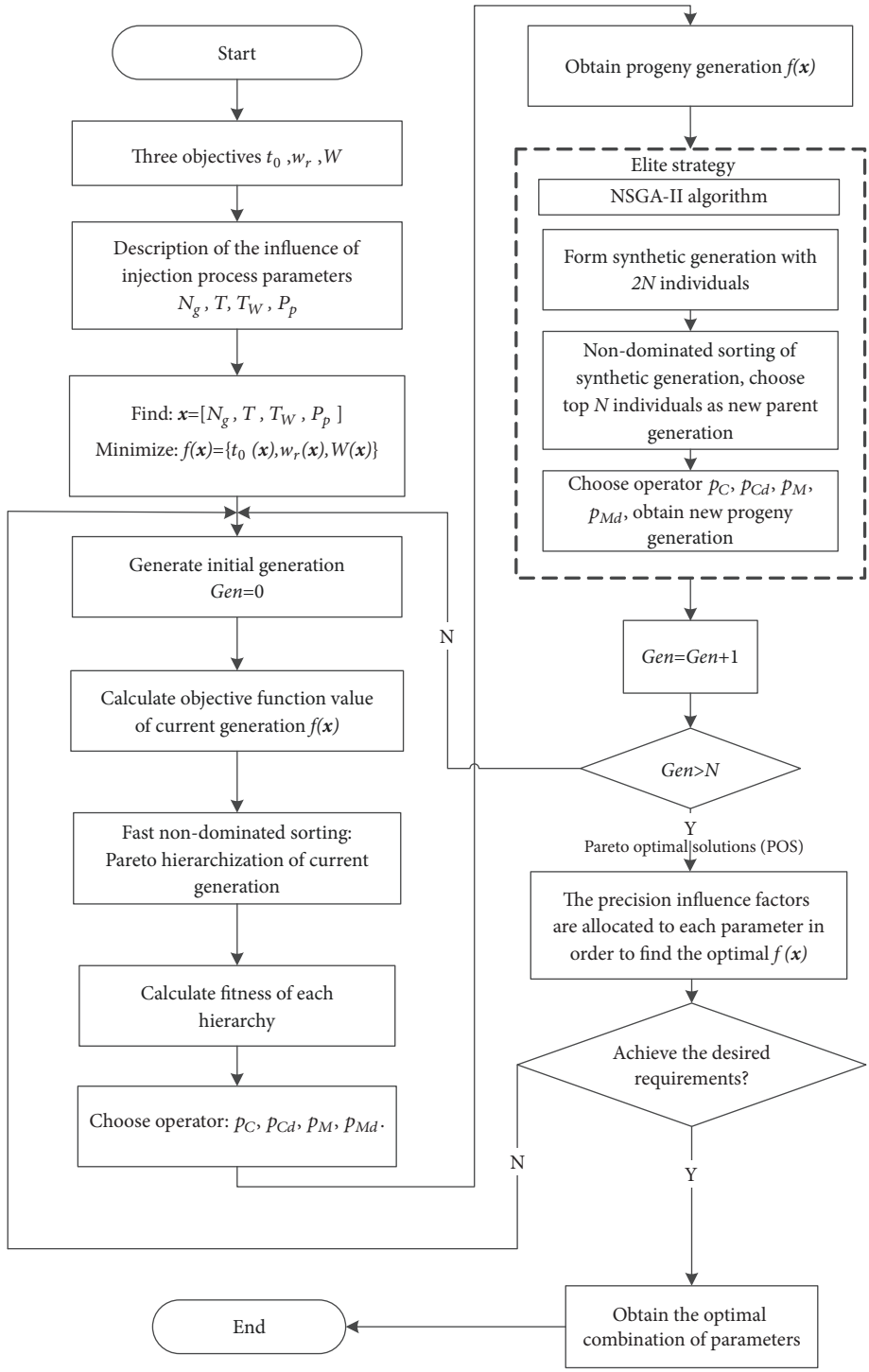

Figure 3: NSGA-II algorithm process.

relatively wide. The three objectives make the optimal solution more complex, and NSGA-II can get the set of Pareto-optimal front frontiers and then select the optimal injection molding process parameters. Operational parameters used in NSGA-II are listed in Table 7. The optimization process is shown in Figure 4; Figure 4(a) shows the initial set of solutions and Figure 4(b) shows the Pareto-optimal set for the three objectives using NSGA-II. A set of Pareto-optimal solutions (POS) using NSGA-II is listed in Table 8. Three candidate schemes are selected according to the predefined parameters in initial hierarchy and optimized parameters using NSGA-II in periodical hierarchy.

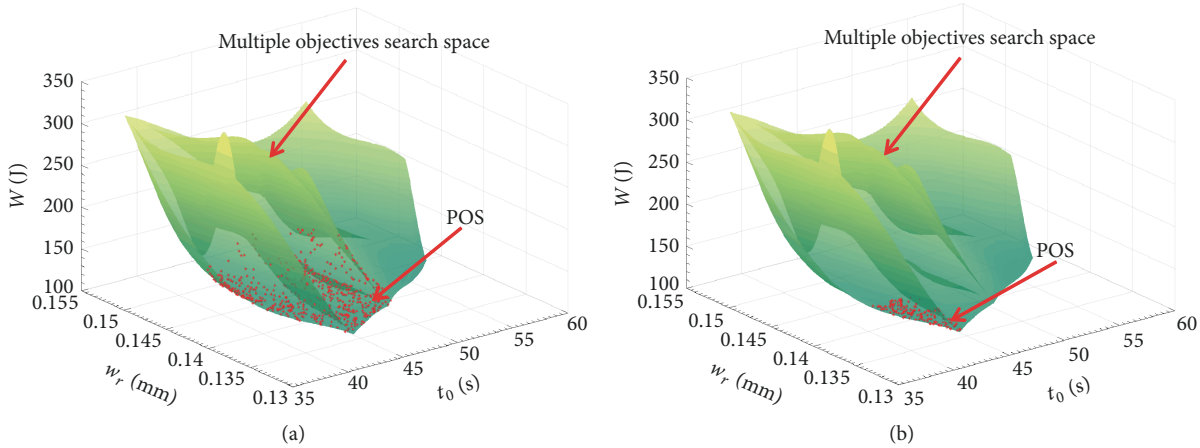

Figure 4: Hierarchy search for the POS process. (a) Initial set of solutions. (b) Pareto-optimal set for the three objectives.

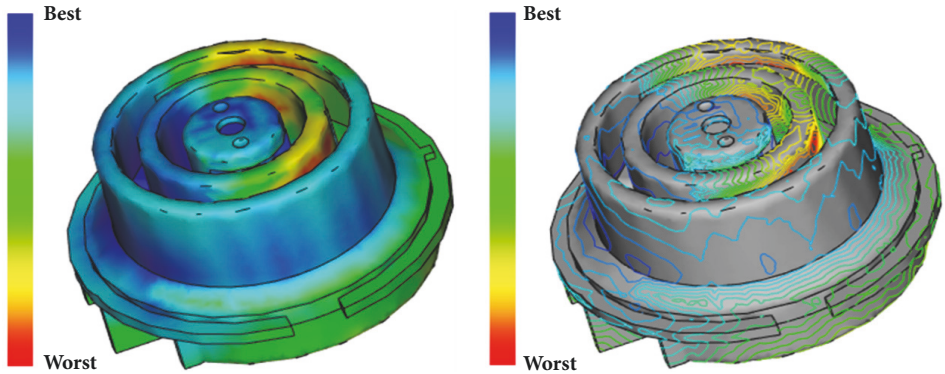

Figure 5: Gate location analysis: (a) shows the shadow map of gate location; (b) shows the contour map of gate location.

Table 7: Operational parameters used in NSGA-II.

NSGA-II Parameters	Values
Population size M	500
Number of generations N	400
Crossover probability p_c	0.8
Crossover distribution index p_{cd}	10
Mutation probability p_M	0.25
Mutation distribution index p_{Md}	20

4. Mold Flow Analysis Comparison of Candidate Schemes in Ultimate Hierarchy

In ultimate hierarchy, three candidate schemes are compared on multiple objectives to determine the final energy-efficient enhancement scheme. Taking temperature controller for example, it is a series of automatic control elements, which are physically deformed in the switch according to the temperature change of the working environment, resulting in some special effects, resulting in conduction or disconnection which can control the operation of the equipment. Temperature controller is mainly used in various high and low voltage switchgear, dry transformer, box type substation, and other related temperature use fields used by the power department. Temperature controller part has complex structure with thin-walled structure, boss and grooves, exquisite design, light quality, high precision, high forming tolerance grade, and more energy consumption. The mold flow analysis of the temperature controller part is mainly carried out.

4.1. Gate Location Comparison. The selection of product materials is ABS, and the analysis type is chosen as the gate location. The final analysis results, as shown in Figure 5, show that different color regions represent different matches, in which the blue region is the best gate location area.

4.2. Gating System Design. The selection of gate position has an important influence on the quality of the molded products. According to gate matching characteristics and location of product structure design gate (Figure 5), different design options were initially selected, which are single gate (Figure 6(a) Scheme 1), double gates (Figure 6(b) Scheme 2), and four gates (Figure 6(c) Scheme 3), as shown in Figures 6(a), 6(b), and 6(c).

Table 8: A set of POSs using NSGA-II.

Candidate Schemes	Injection molding process parameters						
	Optimized parameters using NSGA-II				Predefined parameters		
	N_g	T	T_W	P_p	P_{in}	t_p	t_c
Scheme 1	1	235	50	85	120	10	15
Scheme 2	2	240	53	95	120	10	15
Scheme 3	4	238	52	98	120	10	15

According to the size of products to determine the channel size. In Scheme 1 in the submarine gate, sprue small end diameter is Φ4mm, outer diameter is Φ6mm, the shunt diameter is Φ5mm, Φ4mm, and gate diameter is Φ1mm. In Scheme 2 using point gate, sprue small end diameter is Φ4mm and outer diameter is Φ6mm. The channel diameter is Φ5mm, another channel for the end cone diameter is Φ4mm, small end diameter is Φ3mm, and gate diameter is Φ1mm; Scheme 3 and Scheme 2 are the same, but there are two more gate locations.

4.3. Thermoplastic Rheomolding Analysis Results. Figures 6(d), 6(e), and 6(f), respectively, indicate the results of the melt filled cavity under different schemes, in which the red area is the final filling of the product. In Figure 6(d) Scheme 1, t_1 is 0.7918s; in Figure 6(b) Scheme 2, t_1 is 0.7509s; in Figure 6(c) Scheme 3, t_1 is 0.8214s. From the time of filling, the three schemes have little difference, and the time of Scheme 2 is the shortest.

Figures 6(g), 6(h), and 6(i), respectively, show the forming time t_0, which includes the time for filling, packing, and cooling. In Figure 6(g) Scheme 1, t_0 is 37.54s; in Figure 6(h) Scheme 2, t_0 is 37.50s; in Figure 6(i) Scheme 3, t_0 is 32.07s. It can be seen that Scheme 3 is the shortest.

Figures 7(a), 7(b), and 7(c), respectively, indicate the flow front temperature T_F of the filling analysis of the product. In Figure 7(a) Scheme 1, T_F is 178.4°C~231.7°C; in Figure 7(b) Scheme 2, T_F is 182.1°C~230.6°C; in Figure 7(c) Scheme 3, T_F is 97.00°C~230.8°C. The temperature difference of Scheme 3 is too large, which is not conducive to the melt flow forming. The temperature difference between Scheme 1 and Scheme 2 is acceptable.

Figures 7(d), 7(e), and 7(f), respectively, indicate bulk temperature T_B. In Figure 7(d) Scheme 1, T_B is 81.48°C~239.0°C; in Figure 7(e) Scheme 2, T_B is 107.0°C~235.6°C; in Figure 7(f) Scheme 3, T_B is 54.08°C~235.4°C. The results show that the maximum T_B does not exceed the degradation temperature of the material and the difference between the T_B in comparison with Scheme 1 and Scheme 3 and Scheme 2 is the smallest.

Figures 7(g), 7(h), and 7(i), respectively, indicate the bulk temperature at end of filling T_E of different schemes. In Figure 7(g) Scheme 1, T_E is 81.48°C~237.9°C; in Figure 7(h) Scheme 2, T_E is 72.9°C~234.9°C; in Figure 7(i) Scheme 3, T_E is 59.40°C~231.9°C. The difference between T_E in comparison with Scheme 2 and Scheme 3 and Scheme 1 is the smallest.

Figures 8(a), 8(b), and 8(c), respectively, show the pressure and speed of filling analysis during the product filling. If there is a grey area in the figure, it indicates that the area is not completely filled when speed/pressure switches. It is evident from Figure 8(a) Scheme 1 that there is an incomplete filling defect in the half part of the product when only one gate exists. The same problems exist in Figure 8(b) Scheme 2 and Figure 8(c) Scheme 3, but the grey areas are smaller than those in the first one (Scheme 1). In the actual production process, we can increase the injection pressure to avoid filling incomplete defects.

Figures 8(d), 8(e), and 8(f), respectively, indicate the warping deformation w_r of the product. In Figure 8(d) Scheme 1, w_r is 0.1335mm; in Figure 8(e) Scheme 2, w_r is 0.1169mm; in Figure 8(f) Scheme 3, w_r is 0.1265mm. It can be seen that Scheme 2 is the smallest.

Figures 8(g), 8(h), and 8(i), respectively, indicate the air traps results of the product. The air traps location of products is mostly located at the edge of products. During the actual injection molding process, gas can be removed through clearance between mold parting surface and forming rod.

Figures 8(j), 8(k), and 8(l), respectively, indicate the results of the distribution of the weld lines of the product. A large number of weld lines will be produced due to the structure of this product. Welding lines are also a product defect, which will reduce the quality of the product surface, so it is compared to Figure 8(j) Scheme 1 and Figure 8(l) Scheme 3, and the weld lines in Figure 8(k) Scheme 2 are less.

4.4. Energy Consumption Comparison of Injection Molding. The volume, pressure, clamp force, and flow rate during filling process are listed in Table 9 (Scheme 2), where status V is velocity control, P is pressure control, V/P is velocity/pressure switch-over, and 1N is 0.000102 tonne force. Take Scheme 2 as an example; energy consumption of injection molding can be calculated according to the injection parameters in the injection process, such as time, pressure, and flow rate.

According to the data in the Table 9, bringing the data into (27), we can get the relationship between t and N_m as shown in Figure 9. By integrating each curve in Figure 9, energy consumption of injection molding W can be obtained. Relative to Scheme 1 and Scheme 3, the energy consumption of Scheme 2 is the smallest.

$$\begin{aligned} W_1 &= 267.9212\ J \\ W_2 &= 155.7913\ J \\ W_3 &= 188.5200\ J \end{aligned} \tag{31}$$

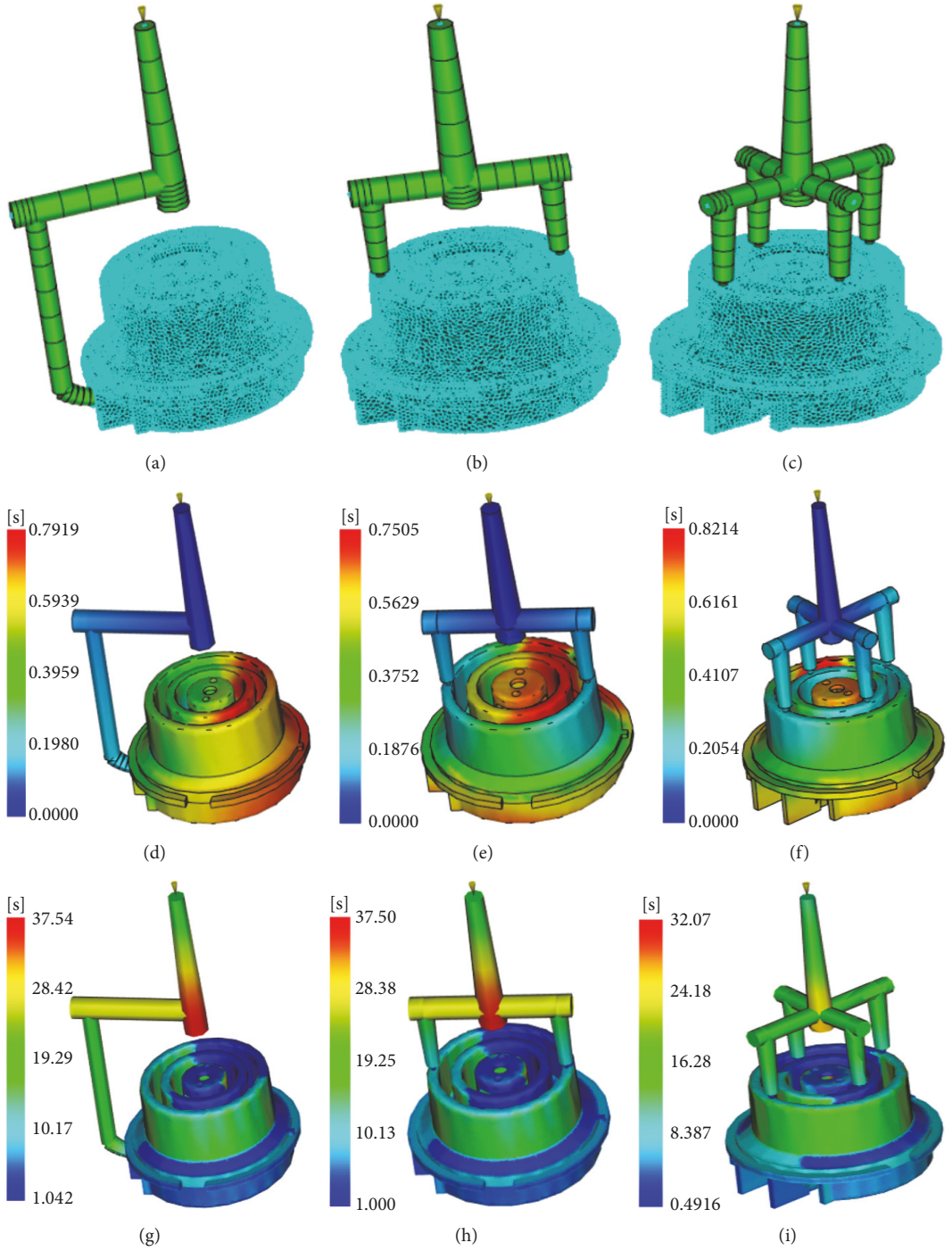

Figure 6: (a), (b), and (c) show three different gating system schemes (Scheme 1, Scheme 2, and Scheme 3); (d), (e), and (f) show the filling time of different schemes (Scheme 1, Scheme 2, and Scheme 3); (g), (h), and (i) show the forming time of different schemes (Scheme 1, Scheme 2, and Scheme 3).

where W_1 is energy consumption of Scheme 1 (J); W_2 is energy consumption of Scheme 2 (J); W_3 is energy consumption of Scheme 3 (J).

4.5. Results Comparison. Polymer extrusion is an energy intensive production process and process energy efficiency has become a key concern in the current industry with the pressure of reducing the global carbon footprint [53]. It is necessary to determine the choice of the scheme from many aspects [54]. According to the previous analysis results, Table 10 can be listed. From the table, you can choose Scheme 2 as the best solution in three schemes, that is,

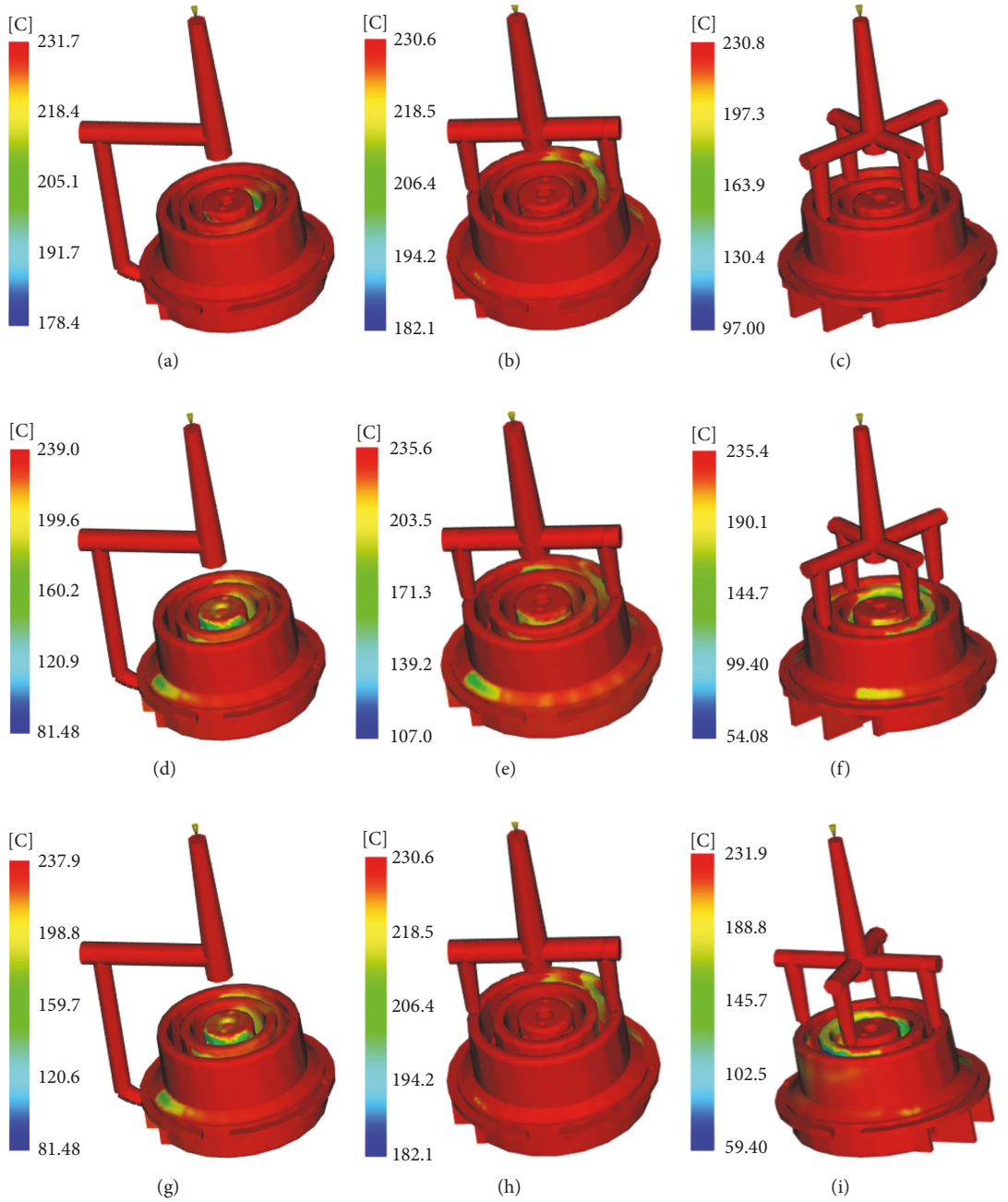

FIGURE 7: (a), (b), and (c) show the flow front temperature of different schemes (Scheme 1, Scheme 2, and Scheme 3); (d), (e), and (f) show the bulk temperature of different schemes (Scheme 1, Scheme 2, and Scheme 3); (g), (h), and (i) show the bulk temperature at end of filling of different schemes (Scheme 1, Scheme 2, and Scheme 3).

select the two gates type. t_1 is optimized (reduced) from 0.8214s (Scheme 3) to 0.7509s (Scheme 2) with ratio of 8.58%; the T_F is optimized (reduced) by 63.75% comparison with Scheme 3; the w_r is optimized (reduced) from 0.1335mm to 0.1169mm with ratio of 14.2%; the R is optimized (increased) from 76.11% (Scheme 3) to 80.78% (Scheme 2) with ratio of 6.14%; the W is optimized (reduced) from 267.9212J (Scheme 1) to 155.7913J (Scheme 2) with ratio of 41.85%.

5. Experimental Verification

The testing machine is JU20000-GJZCJH full hydraulic injection machine with two plates. The parameters are as follows: screw diameter Φ65mm, injection volume 1.1115e7 mm^3, injection weight 10115 g, injection rate 1448 g/s, plasticizing capacity of screws 165 g/s, injection pressure 142 MPa, injection stroke 629 mm, screw speed 0~79 rpm, clamp force 20000 kN, allowable mold size 1800∗1590 mm, allowable

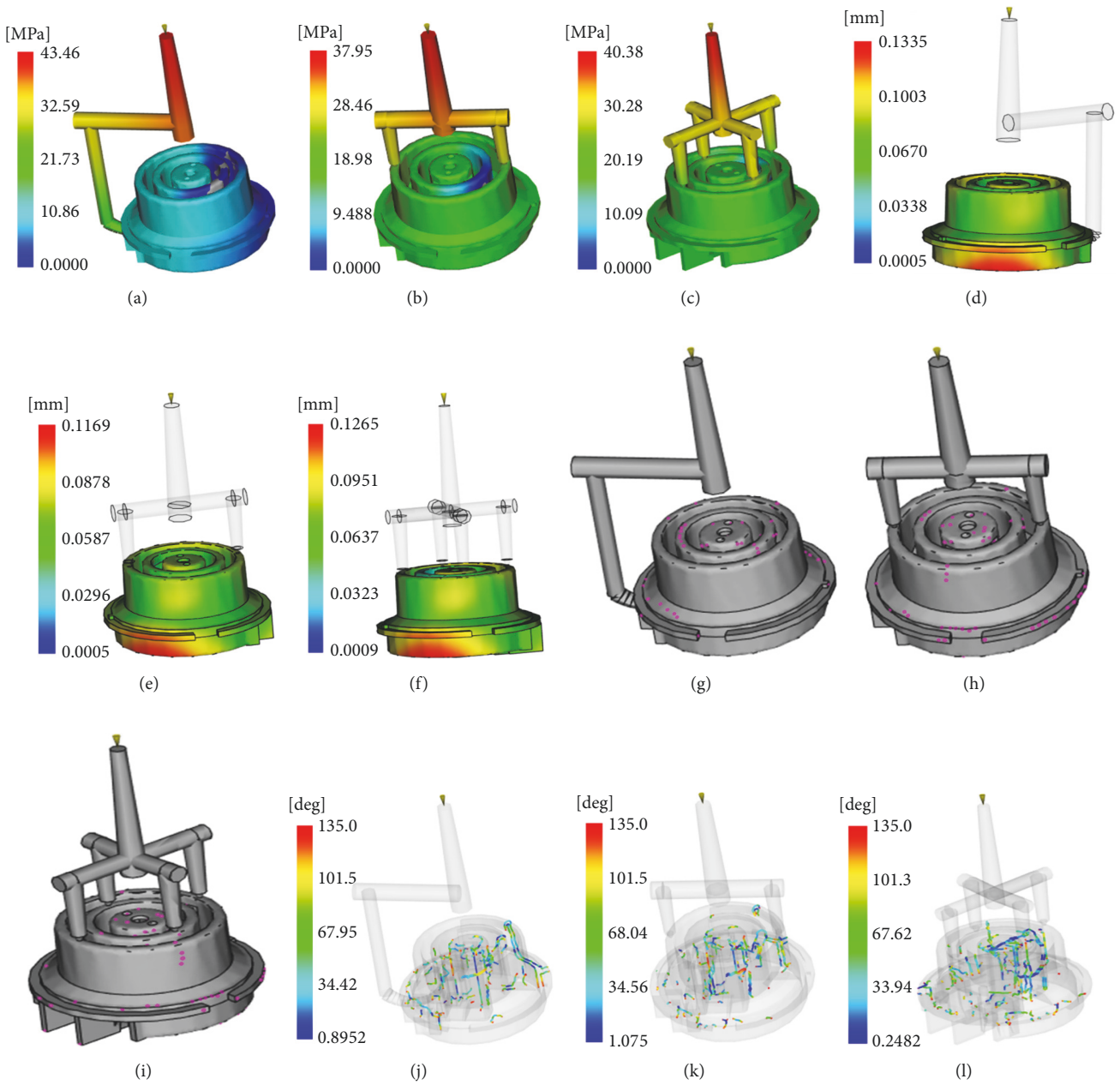

Figure 8: (a), (b), and (c) show the pressure in speed/pressure switching of different schemes (Scheme 1, Scheme 2, and Scheme 3); (d), (e), and (f) show the warping deformation of different schemes (Scheme 1, Scheme 2, and Scheme 3); (g), (h), and (i) show the air traps of different schemes (Scheme 1, Scheme 2, and Scheme 3); (j), (k), and (l) show the weld lines of different schemes (Scheme 1, Scheme 2, and Scheme 3).

mold thickness 800-1600mm, mold opening stroke 1800 mm, and maximum distance between moving and static plate 3400 mm which is shown in Figure 10(a). Figure 10(b) shows the physical comparison before and after multiobjective optimization of temperature controller part. Figure 10(c) and Figure 10(d) show the experimental equipment, respectively.

The experimental results show that the HOO method of improving injection molding parameters is validated. According to the injection molding parameters set in Scheme 2, compared with the original product, the final injection product precision is improved, the amount of warping deformation is greatly reduced, and the thickness uniformity of thin-walled structure is greatly improved.

6. Conclusions

(1) Hierarchy Orthogonal Optimization (HOO) Method to Solve Numerous Heterogeneous Parameters Optimization. The viscoelastic injection molding involves multidisciplinary

Table 9: Scheme 2 volume, pressure, clamp force, flow rate during filling process of valve part.

Time (s)	Volume (%)	Pressure (MPa)	Clamp force F (tonne)	Q ($cm^3 \cdot s^{-1}$)	Status	N_m (W)
0.041	4.96	4.29	0.00	12.51	V	53.6679
0.072	9.09	5.45	0.00	12.55	V	68.3975
0.111	14.46	7.15	0.01	12.52	V	89.518
0.141	18.37	11.09	0.08	11.50	V	127.535
0.177	22.98	14.73	0.15	12.52	V	184.4196
0.212	27.87	15.58	0.16	12.56	V	195.6848
0.247	32.69	16.24	0.18	12.59	V	204.4616
0.283	37.66	16.75	0.19	12.61	V	211.2175
0.318	42.43	17.17	0.21	12.62	V	216.6854
0.354	47.47	17.57	0.22	12.62	V	221.7334
0.390	52.34	18.17	0.25	12.61	V	229.1237
0.424	56.97	18.54	0.28	12.64	V	234.3456
0.460	61.96	18.86	0.30	12.64	V	238.3904
0.495	66.71	19.18	0.32	12.64	V	242.4352
0.531	71.59	19.65	0.35	12.63	V	248.1795
0.566	76.32	20.30	0.40	12.64	V	256.592
0.601	81.09	20.90	0.46	12.65	V	264.385
0.636	85.70	21.53	0.53	12.65	V	272.3545
0.671	90.32	23.40	0.78	12.58	V	294.372
0.706	94.81	26.92	1.24	12.66	V	340.8072
0.742	99.27	31.85	1.96	12.65	V	402.9025
0.750	99.99	37.57	3.00	2.05	P	77.0185
0.750	100.00	37.49	3.01	2.05	Filled	76.8545

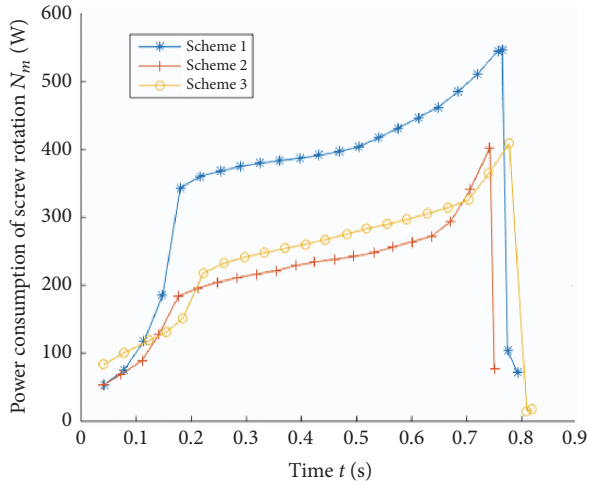

Figure 9: Time-power curve of different design schemes.

thermoplastic rheomolding heterogeneous parameters. It is difficult to implement optimization for the traditional multiobjective optimization. Therefore, hierarchy orthogonal optimization (HOO) method is proposed to solve numerous heterogeneous parameters optimization. The advantage of HOO lies in the fact that it can either extract significant influence parameters from vast heterogeneous parameters or obtain the global Pareto front by optimizing the extracted significant influence parameters in uncertain search space.

(2) Three Hierarchies to Complete Hierarchy Orthogonal Optimization (HOO). In initial hierarchy, through Taguchi orthogonal experiment and Analysis of Variance (ANOVA), the amount of gate, melt temperature, mold temperature, and packing pressure are extracted as the significant influence parameters. In periodical hierarchy, the multiobjective optimization model takes the forming time, warping deformation, and energy consumption of injection molding as the multiple objectives. The NSGA-II (Nondominated Sorting Genetic Algorithm II) optimization is employed to obtain the optimal solution through the global Pareto front. In ultimate hierarchy, three candidate schemes are compared on multiple objectives to determine the final energy-efficient enhancement scheme.

(3) Energy-Efficient Enhancement Is Realized on Forming Time, Warping Deformation, and Energy Consumption.

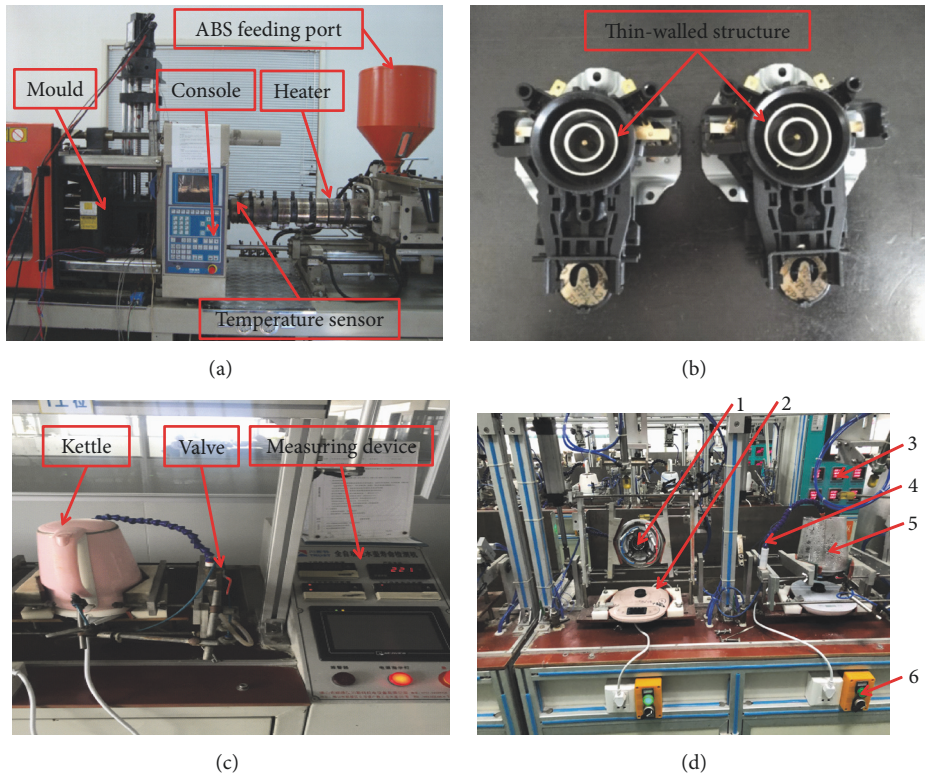

FIGURE 10: (a) Mold and injection molding machine equipment; (b) physical comparison before and after multiobjective optimization; (c) test-bed device; (d) experimental equipment: 1: temperature controller part, 2: device base, 3: temperature display instrument, 4: temperature sensor, 5: experimental vessel, and 6: switch.

TABLE 10: Comparison of results.

Performance parameters	Thermoplastic rheomolding results			Optimal Scheme 2	
	Scheme 1	Scheme 2	Scheme 3	Comparison with scheme 1	Comparison with scheme 3
t_1 (s)	0.7919	0.7509	0.8214	5.18%	8.58%
t_0 (s)	37.54	37.50	32.07	0.11%	-16.93%
T_F (°C)	178.4~231.7	182.1~230.6	97.00~230.8	9.01%	63.75%
T_B (°C)	81.48 ~239.0	107.0~235.6	97.00 ~230.8	18.36%	3.89%
T_E (°C)	81.48 ~237.9	72.9 ~234.9	54.08~235.4	-3.57%	10.30%
P_s (MPa)	43.46	37.95	40.38	12.68%	6.02%
w_r (mm)	0.1335	0.1169	0.1265	14.2%	8.2%
M_0 (g)	8.8587	8.6775	9.2443	2.05%	6.13%
M_1 (g)	6.9737	7.0020	7.0361	-0.41%	0.48%
M_2 (g)	1.8499	1.6755	2.2082	9.43%	24.12%
R	78.72%	80.78%	76.11%	-2.62%	-6.14%
V_0 (cm3)	9.1544	8.9424	9.4682	2.32%	5.55%
V_2 (cm3)	1.8789	1.6668	2.1927	11.29%	23.98%
W (J)	267.9212	155.7913	188.5200	41.85%	17.36%

Energy-efficient multiobjective optimization for injection molding process is realized using integrated injection molding part design, mold design, processing equipment and process control, and material selection. A typical temperature controller part is analyzed and the injection molding energy consumption is reduced by 41.85%. Through the physical experiment of injection process, the proposed method is further verified.

Nomenclature

a: The measure of degree of the shear-thinning behavior
A_1: Effective area of hydraulic cylinder (cm^{-2})
$\boldsymbol{b}$: Temperature at the last time and the heat source related to the convection heat transfer and the viscous heat (°C)
C: Volume efficiency of hydraulic pump
C_1: Viscous damping coefficient of hydraulic cylinder ($N{\cdot}s{\cdot}cm^{-1}$)
C_p: Specific heat capacity ($J{\cdot}kg^{-1}\cdot{}^{\circ}C^{-1}$)
D: Screw diameter (cm)
$\mathrm{v}f(\boldsymbol{x})$: Objective function $\{t_0(\boldsymbol{x}), w_r(\boldsymbol{x}), W(\boldsymbol{x})\}$ considering parameters $\boldsymbol{x}$ of injection process
F: Clamping force (N)
F_L: Load resistance (N)
g_x, g_y, g_z: Acceleration of gravity in x, y, z direction ($m{\cdot}s^{-2}$)
H: Displacement of hydraulic cylinder (cm)
i: Node sequence
j: Corresponding node position
k: Thermal conductivity ($W{\cdot}m^{-1}\cdot{}^{\circ}C^{-1}$)
k_e: Load elastic coefficient ($N{\cdot}cm^{-1}$)
$\boldsymbol{K}$: Stiffness matrix
K: Volume modulus of hydraulic fluid (MPa)
L: Screw metering stroke (cm)
m, h, A_1, A_2, E_1, E_2: Constants
M: Population size
$\boldsymbol{M_a}$: Coefficient matrix
M_0: Total mass (g)
M_1: Total weight of parts (g)
M_2: Main stream/runner/gate total weight (g)
M_E: Equivalent mass of hydraulic cylinder (Kg)
M_n: Screw torque (N·m)
n: Iteration step
$\boldsymbol{N}$: Number of generations
N_g: The amount of gate
N_j: Linear interpolating function
N_m: Power consumption of screw rotation (W)
N_s: Motor speed ($r{\cdot}min^{-1}$)
p_C: Crossover probability
p_{Cd}: Crossover distribution index
p_M: Mutation probability
p_{Md}: Mutation distribution index
P: Pressure (MPa)
P_1: Hydraulic pressure (MPa)
P_j: Node pressure in trigonometric unit (MPa)
P_p: Packing pressure (MPa)
P_s: Pressure in speed/pressure switching (MPa)
q_1: Hydraulic fluid flow ($cm^3{\cdot}s^{-1}$)
Q: Flow rate ($cm^3{\cdot}s^{-1}$)
Q_c: Internal calorific (J)
r: Screw speed ($r{\cdot}min^{-1}$)
SN: Material utilization ratio
t: Time (s)
t_0: Forming time (s)
t_1: Filling time (s)
t_c: Cooling time (s)
t_p: Packing time (s)
T: Melt temperature (°C)
T_0: Temperature of injection (°C)
T_B: Bulk temperature (°C)
T_E: Bulk temperature at end of filling (°C)
T_F: Flow front temperature (°C)
T_w: Mold temperature (°C)
T^i: T_F of a certain moment (°C)
$\boldsymbol{T^{n+1}}$: Temperature of node at new time (°C)
u, v, w: Component of velocity vector V in x, y, z direction ($m{\cdot}s^{-1}$)
v_i: Injection speed ($cm{\cdot}s^{-1}$)
V: Rated displacement of a quantitative pump ($cm^3{\cdot}s^{-1}$)
V_0: Total volume (cm^3)
V_1: Cavity volume of part (cm^3)
V_2: Main channel/runner/gate volume to be filled (cm^3)
V_3: Part volume after cooling (cm^3)
V_4: Total volume of front and rear of hydraulic cylinder (cm^3)
V_s: Volumetric shrinkage
w_r: Warping deformation (mm)
W: Energy consumption of injection molding (J)
W_1: Energy consumption of Scheme 1 (J)
W_2: Energy consumption of Scheme 2 (J)
W_3: Energy consumption of Scheme 3 (J)
$\boldsymbol{x}$: Parameters of injection process, including N_g, T, T_W, P_p
Y_i: Experimental result
α: The degree of cure (0, 1)
$\dot{\gamma}$: Strain rate tensor intensity(s^{-1})
η: Kinetic viscosity of the material (Pa·s)
η_0: Zero shear-rate kinetic viscosity (Pa·s)
λ: Total leakage coefficient of hydraulic cylinder
ρ: Melt density of material ($g{\cdot}cm^{-3}$)
ρ_s: Solid density of materials ($g{\cdot}cm^{-3}$)
$\boldsymbol{\sigma}$: Total stress (MPa)
τ^*: The critical shear-stress that is need to transform the melt flow from the Newtonian to shear-thinning or power-law behavior (Pa)
∇: Hamilton operator.

Data Availability

The data used to support the findings of this study are available from the corresponding author upon request.

Conflicts of Interest

The authors declare that they have no conflicts of interest.

Acknowledgments

The work presented in this article is funded by the National Natural Science Foundation of China (nos. 51775494 and 51521064), National Science and Technology Major Project of China (no. 2015ZX04014021), Science and Technology Plan Project of Zhejiang Province (2017C31002), and Fundamental Research Funds for the Central Universities (2017FZA4003). Thanks are due to YANG Fujian which is a R&D manager in Joyoung Company Limited, Zhejiang, China, for the help in the rheomolding experiment.

References

[1] J. Madan, M. Mani, and K. W. Lyons, "Characterizing Energy Consumption of the Injection Molding Process," in *Proceedings of the ASME 2013 International Manufacturing Science and Engineering Conference collocated with the 41st North American Manufacturing Research Conference*, Madison, WI, USA.

[2] R. E. Khayat, W. Elsin, and K. Kim, "An adaptive boundary element approach to transient free surface flow as applied to injection molding," *International Journal for Numerical Methods in Fluids*, vol. 33, no. 6, pp. 847–868, 2015.

[3] B. J. Araújo, J. C. Teixeira, A. M. Cunha, and C. P. Groth, "Parallel three-dimensional simulation of the injection molding process," *International Journal for Numerical Methods in Fluids*, vol. 59, no. 7, pp. 801–815, 2010.

[4] K. Kwon, A. I. Isayev, and K. H. Kim, "Toward a viscoelastic modeling of anisotropic shrinkage in injection molding of amorphous polymers," *Journal of Applied Polymer Science*, vol. 98, no. 5, pp. 2300–2313, 2010.

[5] J. Yang, Y. Jia, Y. Ding, H. He, T. Shi, and L. An, "Edge effect in RTM processes under constant pressure injection conditions," *Journal of Applied Polymer Science*, vol. 118, no. 2, pp. 1014–1019, 2010.

[6] M. H. Chiang, Y. P. Yeh, F. L. Yang, and Y. N. Chen, "Integrated control of clamping force and energy-saving in hydraulic injection moulding machines using decoupling fuzzy sliding-mode control," *The International Journal of Advanced Manufacturing Technology*, vol. 27, no. 1-2, pp. 53–62, 2005.

[7] C. Chu, J. Wei, and M. Shih, "Adaptive model following control of the mold filling process in an injection molding machine," *Polymer Engineering & Science*, vol. 31, no. 15, pp. 1123–1129, 1991.

[8] Y. Peng and W. Wei, "Application and control strategy of servo motor driven constant pump hydraulic system in precision injection molding," *Jixie Gongcheng Xuebao/Journal of Mechanical Engineering*, vol. 47, no. 2, pp. 173–179, 2011.

[9] Y. Xu, H. Lu, T. Gao, and W. Zhang, "Predicting the low-velocity impact behavior of polycarbonate: Influence of thermal history during injection molding," *International Journal of Impact Engineering*, vol. 86, pp. 265–273, 2015.

[10] M. Huang, J. Yu, and Y. Lin, "Effect of rapid mold surface inducting heating on the replication ability of microinjection molding light-guided plates with V-grooved microfeatures," *Journal of Applied Polymer Science*, vol. 118, no. 5, pp. 3058–3065, 2010.

[11] D. Kusić, T. Kek, J. M. Slabe, R. Svečko, and J. Grum, "The impact of process parameters on test specimen deviations and their correlation with AE signals captured during the injection moulding cycle," *Polymer Testing*, vol. 32, no. 3, pp. 583–593, 2013.

[12] A. Fernandez, M. Muniesa, and C. Javierre, "In-line rheological testing of thermoplastics and a monitored device for an injection moulding machine: Application to raw and recycled polypropylene," *Polymer Testing*, vol. 33, pp. 107–115, 2014.

[13] J. Vera-Sorroche, A. L. Kelly, E. C. Brown et al., "The effect of melt viscosity on thermal efficiency for single screw extrusion of HDPE," *Chemical Engineering Research and Design*, vol. 92, no. 11, pp. 2404–2412, 2014.

[14] C.-C. Tsai, S.-M. Hsieh, and H.-E. Kao, "Mechatronic design and injection speed control of an ultra high-speed plastic injection molding machine," *Mechatronics*, vol. 19, no. 2, pp. 147–155, 2009.

[15] M. Studer and F. Ehrig, "Numerical shape optimization as an approach to reduce material waste in injection molding," *The International Journal of Advanced Manufacturing Technology*, vol. 78, no. 9-12, pp. 1557–1571, 2015.

[16] M. G. H. M. Baltussen, M. A. Hulsen, and G. W. M. Peters, "Numerical simulation of the fountain flow instability in injection molding," *Journal of Non-Newtonian Fluid Mechanics*, vol. 165, no. 11-12, pp. 631–640, 2010.

[17] S. Kanagalakshmi, D. Manamalli, and M. Mohamedrafiq, "Implementation of multimodel-based PID and intelligent controller for simulated and real-time temperature control of injection molding machine," *Chemical Engineering Communications*, vol. 203, no. 4, pp. 452–462, 2015.

[18] J.-R. Shie, "Optimization of injection-molding process for mechanical properties of polypropylene components via a generalized regression neural network," *Polymers for Advanced Technologies*, vol. 19, no. 1, pp. 73–83, 2008.

[19] M. Zhai, Y. Lam, and C. Au, "Gate location optimization scheme for plastic injection molding," *e-Polymers*, vol. 9, no. 1, 2009.

[20] J. Liu, X. Chen, Z. Lin, and S. Diao, "Multiobjective optimization of injection molding process parameters for the precision manufacturing of plastic optical lens," *Mathematical Problems in Engineering*, vol. 2017, Article ID 2834013, 13 pages, 2017.

[21] J. Xu and S. Zhang, "Shape retrieval method of 3D models based on shape-distribution graph and BP neural network," *Zhejiang Daxue Xuebao (Gongxue Ban)/Journal of Zhejiang University (Engineering Science)*, vol. 43, no. 5, pp. 877–883, 2009.

[22] J. Xu and S. Zhang, "3D shape and structure retrieval method of mechanical parts based on recursive segmentation," *Jixie Gongcheng Xuebao/Journal of Mechanical Engineering*, vol. 45, no. 11, pp. 176–183, 2009.

[23] S. Zhang and J. Xu, "Acquisition and active navigation of knowledge particles throughout product variation design process," *Chinese Journal of Mechanical Engineering*, vol. 22, no. 3, pp. 395–402, 2009.

[24] J. Xu, S. Zhang, J. Tan, and X. Liu, "Non-redundant tool trajectory generation for surface finish machining based on geodesic curvature matching," *The International Journal of Advanced Manufacturing Technology*, vol. 62, no. 9-12, pp. 1169–1178, 2012.

[25] J. Xu, S. Zhang, J. Tan, and H. Sheng, "Interruption performance design of variable freedom mechanism triggered by electro-mechanical-magnetic coupling," *Proceedings of the Institution of Mechanical Engineers, Part C: Journal of Mechanical Engineering Science*, vol. 231, no. 18, pp. 3330–3341, 2017.

[26] J. Xu, X. Chen, S. Zhang, Q. Chen, H. Gou, and J. Tan, "Thermal design of large plate-fin heat exchanger for cryogenic air separation unit based on multiple dynamic equilibriums," *Applied Thermal Engineering*, vol. 113, pp. 774–790, 2017.

[27] S. Zhang, J. Xu, H. Gou, and J. Tan, "A Research Review on the Key Technologies of Intelligent Design for Customized Products," *Engineering Journal*, vol. 3, no. 5, pp. 631–640, 2017.

[28] A. I. Isayev and C. A. Hieber, "Toward a viscoelastic modelling of the injection molding of polymers," *Rheologica Acta*, vol. 19, no. 2, pp. 168–182, 1980.

[29] R. E. Nickell, R. I. Tanner, and B. Caswell, "The solution of viscous incompressible jet and free-surface flows using finite-element methods," *Journal of Fluid Mechanics*, vol. 65, no. 1, pp. 189–206, 2006.

[30] Y. Dimakopoulos, "An efficient parallel and fully implicit algorithm for the simulation of transient free-surface flows of multimode viscoelastic liquids," *Journal of Non-Newtonian Fluid Mechanics*, vol. 165, no. 7-8, pp. 409–424, 2010.

[31] M. Hadid, S. Rechak, and A. Zouani, "Empirical nonlinear viscoelastic model for injection molded thermoplastic composite," *Polymer Composites*, vol. 23, no. 5, pp. 771–778, 2010.

[32] D. Pettas, G. Karapetsas, Y. Dimakopoulos, and J. Tsamopoulos, "On the origin of extrusion instabilities: linear stability analysis of the viscoelastic die swell," *Journal of Non-Newtonian Fluid Mechanics*, vol. 224, pp. 61–77, 2015.

[33] S. Tsouka, Y. Dimakopoulos, V. Mavrantzas, and J. Tsamopoulos, "Stress-gradient induced migration of polymers in corrugated channels," *Journal of Rheology*, vol. 58, no. 4, pp. 911–947, 2014.

[34] Y. Dimakopoulos and J. Tsamopoulos, "On the transient coating of a straight tube with a viscoelastic material," *Journal of Non-Newtonian Fluid Mechanics*, vol. 159, no. 1-3, pp. 95–114, 2009.

[35] Y. Dimakopoulos and J. Tsamopoulos, "Gas-assisted injection molding with fluids partially occupying straight or complex tubes," *Polymer Engineering & Science*, vol. 46, no. 1, pp. 47–68, 2006.

[36] N. Al-Rawahi and G. Tryggvason, "Numerical simulation of dendritic solidification with convection: Three-dimensional flow," *Journal of Computational Physics*, vol. 194, no. 2, pp. 677–696, 2004.

[37] Y. K. Shen and W. Y. Wu, "Analysis of the three-dimensional micro-injection molding," *International Communications in Heat & Mass Transfer*, vol. 29, no. 3, pp. 423–431, 2002.

[38] H. H. Chiang, C. A. Hieber, and K. K. Wang, "A unified simulation of the filling and postfilling stages in injection molding. Part I: Formulation," *Polymer Engineering & Science*, vol. 31, no. 2, pp. 116–124, 1991.

[39] K. M. Choudhary, P. Seshadri, and J. Bae, "Melt temperature profile prediction for thermoplastic injection molding," *Polymer Engineering & Science*, vol. 39, no. 9, pp. 1787–1801, 1999.

[40] W.-J. Chang, H.-Y. Qiao, and C.-C. Ku, "Sliding mode fuzzy control for nonlinear stochastic systems subject to pole assignment and variance constraint," *Information Sciences*, vol. 432, pp. 133–145, 2018.

[41] R.-E. Precup, M.-B. Radac, R.-C. Roman, and E. M. Petriu, "Model-free sliding mode control of nonlinear systems: Algorithms and experiments," *Information Sciences*, vol. 381, pp. 176–192, 2017.

[42] H. Li, P. Shi, and D. Yao, "Adaptive sliding mode control of markov jump nonlinear systems with actuator faults," *IEEE Transactions on Automatic Control*, vol. 62, no. 4, pp. 1933–1939, 2017.

[43] F. Li, H. Cheng, G. Wang, R. Bai, and L. Lu, "The effect of plasticizing parameters on the energy consumption of injection molding machine," *Engineering Plastics Application*, vol. 39, no. 6, pp. 44–47, 2011.

[44] M.-T. Chuang and Y.-K. Yang, "Simulation study on optimization of injection molding process for thin-shell plastic parts via the taguchi method and grey relational analysis," *International Polymer Processing*, vol. 24, no. 1, pp. 51–58, 2009.

[45] A. T. Sidambe, I. A. Figueroa, H. G. C. Hamilton, and L. Todd, "Taguchi optimization of mim titanium sintering," *International Journal of Powder Metallurgy*, vol. 47, no. 6, pp. 21–28, 2011.

[46] K. Deb, A. Pratap, S. Agarwal, and T. Meyarivan, "A fast and elitist multiobjective genetic algorithm: NSGA-II," *IEEE Transactions on Evolutionary Computation*, vol. 6, no. 2, pp. 182–197, 2002.

[47] Z. Wei, Y. Feng, J. Tan, J. Wang, and Z. Li, "Multi-objective performance optimal design of large-scale injection molding machine," *The International Journal of Advanced Manufacturing Technology*, vol. 41, no. 3-4, pp. 242–249, 2009.

[48] C. Zhang and X. Ma, "NSGA-II algorithm with a local search strategy for multiobjective optimal design of dry-type air-core reactor," *Mathematical Problems in Engineering*, vol. 2015, Article ID 839035, 9 pages, 2015.

[49] Y. Yang, Z. Wang, B. Yang, Z. Jing, and Y. Kang, "Multiobjective optimization for fixture locating layout of sheet metal part using sVR and NSGA-II," *Mathematical Problems in Engineering*, vol. 2017, Article ID 7076143, 10 pages, 2017.

[50] A. Demissie, W. Zhu, and C. T. Belachew, "A multi-objective optimization model for gas pipeline operations," *Computers & Chemical Engineering*, vol. 100, pp. 94–103, 2017.

[51] S. Jiang and S. Yang, "A strength pareto evolutionary algorithm based on reference direction for multiobjective and many-objective optimization," *IEEE Transactions on Evolutionary Computation*, vol. 21, no. 3, pp. 329–346, 2017.

[52] S. Sanaye and H. Hajabdollahi, "Thermal-economic multi-objective optimization of plate fin heat exchanger using genetic algorithm," *Applied Energy*, vol. 87, no. 6, pp. 1893–1902, 2010.

[53] C. Abeykoon, A. L. Kelly, E. C. Brown, and P. D. Coates, "The effect of materials, process settings and screw geometry on energy consumption and melt temperature in single screw extrusion," *Applied Energy*, vol. 180, pp. 880–894, 2016.

[54] P. F. Rios, A. Ophir, S. Kenig, R. Efrati, L. Zonder, and R. Popovitz-Biro, "Impact of injection-molding processing parameters on the electrical, mechanical, and thermal properties of thermoplastic/carbon nanotube nanocomposites," *Journal of Applied Polymer Science*, vol. 120, no. 1, pp. 70–78, 2011.